Anisotropic magnetoresistance and planar Hall effect in (001) and (111) $LaVO_3/SrTiO_3$ heterostructures

Ruchi Tomar, Sonali Kakkar, Chandan Bera,* and S. Chakraverty†
Nanoscale Physics and Device Laboratory, Institute of Nano Science and Technology, Phase-10, Sector-64, Mohali, Punjab 160062, India

(Received 14 October 2020; revised 16 February 2021; accepted 16 February 2021; published 4 March 2021)

A two-dimensional electron gas at the interfaces of perovskite oxides has unfolded various emergent phenomena. In this work, we fabricate the conducting interface between $LaVO_3$ (LVO) and $SrTiO_3$ (STO) with two different orientations, (001) and (111), employing a pulsed laser deposition system. A signature of weak antilocalization is observed in the (111)-oriented LVO/STO heterostructure which was not present in the (001) heterostructure. We report the observation of a planar Hall effect (PHE) and anisotropic magnetoresistance (AMR) for both heterointerfaces. The AMR and PHE are measured by driving a current I in the plane of the interface and applying an external magnetic field B in the same plane. The angular dependence (angle ϕ between B and I) of AMR and PHE in both cases is observed to be sensitive to applied magnetic field and temperature. The (001)-oriented heterointerface shows larger AMR ($\sim$60%) than (111) ($<$10%), which is the highest among previously reported oxide heterostructures. The PHE shows twofold symmetry as a function of ϕ for both interfaces, and the symmetry remains for all the magnetic field values. In contrast, the AMRs for (001) and (111) have different symmetries. At the same time, they have strong dependence on B. A detailed analysis of our results and density functional theory calculations suggests that the origin of these oscillations (AMR and PHE) observed in (001)- and (111)-oriented LVO/STO interfaces can be linked to their unique Fermi surface reconstruction due to its orbital occupancy and polarization/hybridization.

DOI: 10.1103/PhysRevB.103.115407

I. INTRODUCTION

Low-dimensional electronic systems at the interface of perovskite oxides have shown their potential for spintronic applications such as the spin Hall effect, spin field effect transistors with gate tunable Rashba field, etc. [1–4]. A variety of novel electronic behaviors has also been observed at these interfaces. These interfaces exhibit emergent properties such as two-dimensional electron gases, spin-orbit coupling, orbital properties, magnetism, superconductivity, the coexistence of magnetism with superconductivity, Rashba spin splitting, and so on [5–15]. Two of the interesting phenomena recently observed at these interfaces are anisotropic magnetoresistance (AMR) and the planar Hall effect (PHE). Usually, such effects were observed either in ferromagnetic materials or in topological materials such as topological insulators, Weyl fermions, etc., and are known to arise from different origins [16–30]. In ferromagnetic materials, these effects arise due to the interaction between magnetization and charge transport, whereas in the case of topological materials, their origin is linked to the chiral anomaly present in these systems. The AMR and PHE were also observed at the $LaAlO_3/SrTiO_3$ (LAO/STO) interface and were correlated with the influence of the confinement potential on orbital occupancy as well as spin-orbit interaction [31–38]. Interplay between carrier confinement and possible localized magnetization is proposed that depends on the strength of the applied magnetic field and temperature. These effects (AMR and PHE) were also found to be tuned with gate voltage and carrier concentration [31,32]. It was also demonstrated that the shape of the Fermi surface and carrier effective mass play a crucial role in such observed phenomena [37,39].

The interface of LAO and STO with different orientations [(001), (110), and (111)] had already been reported to show such effects, i.e., PHE and AMR. It is evident that at the LAO/STO interface, the coupling between itinerant electronic bands at the interface and the interface orientation play a crucial role in observed PHE and AMR [31–34,39]. Recently, a new conducting polar-polar interface of $LaVO_3$ (LVO) and $KTaO_3$ (KTO) was also reported to exhibit PHE and AMR, which was explained as being a consequence of strong spin-orbit coupling and Rashba spin splitting. The observed data were explained with a phenomenological model with Rashba spin splitting [14].

In the case of LAO/STO systems conductivity originating from the oxygen vacancy is a major issue. There are two prime reasons for the oxygen vacancy in LAO/STO systems. The growth condition of the LAO thin film is rather reducing (typically, 750 °C). Further, Al has an affinity for oxygen that leads to the creation of the oxygen vacancy in STO. On the other hand, the advantages of LVO/STO are that this heterostructure is prepared in much less reduced growth conditions (600 °C) [6,40]. In addition, V has less affinity for oxygen than Al. We have performed x-ray photoemission spectroscopy that suggests the absence of a detectable oxygen vacancy in the system [6,41]. But this interface of LVO/STO is less explored than LAO/STO and should be investigated more to discover such underlying interesting phenomena.

*chandan@inst.ac.in
†suvankar.chakraverty@inst.ac.in

In this paper, we demonstrate the observation of AMR and PHE at the conducting interface of a Mott insulator (LVO) and a band insulator (STO) with orientations (001) and (111). The (111) interface of LVO/STO shows a signature of spin-orbit coupling. Fourfold and sixfold oscillations in AMR were observed in (001) and (111) LVO/STO interfaces, respectively, whereas PHE for both interfaces remains twofold in nature. In addition, a strong effect of magnetic field and temperature on the AMR and PHE was also observed. Theoretical calculations along with our experimental data suggest that the orbital occupancy and polarization or hybridization as well as the structural change in the Fermi surface in (001) and (111) LVO/STO interfaces lead to the emergence of the oscillations in longitudinal (AMR) and transverse (PHE) resistances for both interfaces.

II. EXPERIMENTAL DETAILS

For this study, the eight monolayers of LVO films were grown on (001)- and (111)-oriented single-terminated STO substrates, using a pulsed laser deposition system. High-temperature annealing followed by deionized-water etching was used to realize single-terminated surfaces of the substrates [42]. The details of the fabrication of these heterostructures are discussed in our previous work [6]. The growth quality and film thickness were monitored by an *in situ* reflection high-energy electron diffraction technique. The growth-related details are given in the Supplemental Material (Fig. S1) [43]. All the electrical as well as magnetotransport characterizations were carried out using a physical property measurement system (PPMS; Dynacool, Quantum Design, 14 T). The angular dependence of the magnetotransport measurements was performed at different magnetic field and temperature values using a horizontal rotator assisted by the PPMS, enabling us to perform angle-dependent measurements. The electrical contacts were made with the help of an ultrasonic wire bonder.

III. RESULTS AND DISCUSSION

A schematic representation of the LVO/STO heterostructure is shown in Fig. 1(a), displaying the alternating planes in LVO and STO with (001) orientation. The alternating planes in (001)-oriented STO are $[TiO_2]^0$ and $[SrO]^0$, and for LVO, the planes are $[LaO]^{+1}$ and $[VO_2]^{-1}$. In Fig. 1(b), the perpendicular (left, B is applied normal to the current plane) and planar (right, B is applied in the current plane) geometries of the measurements are depicted for (001)-oriented LVO/STO heterostructure. A monotonic decrease in sheet resistance was observed down to low temperature, suggesting the conducting nature of the (001)-oriented LVO/STO interface. Recently, we used photoluminescence spectroscopy and time-correlated photon counting combined with electrical measurements to reveal the distribution of the carriers in the LVO/STO interface. That suggests the quasi-two-dimensional nature of the conducting electrons at LVO/STO interfaces, similar to what was reported for LAO/STO heterointerfaces [44–48]; the details are beyond the scope of the present paper. The carrier density and mobility of this heterostructure were extracted from conventional Hall measurements and were

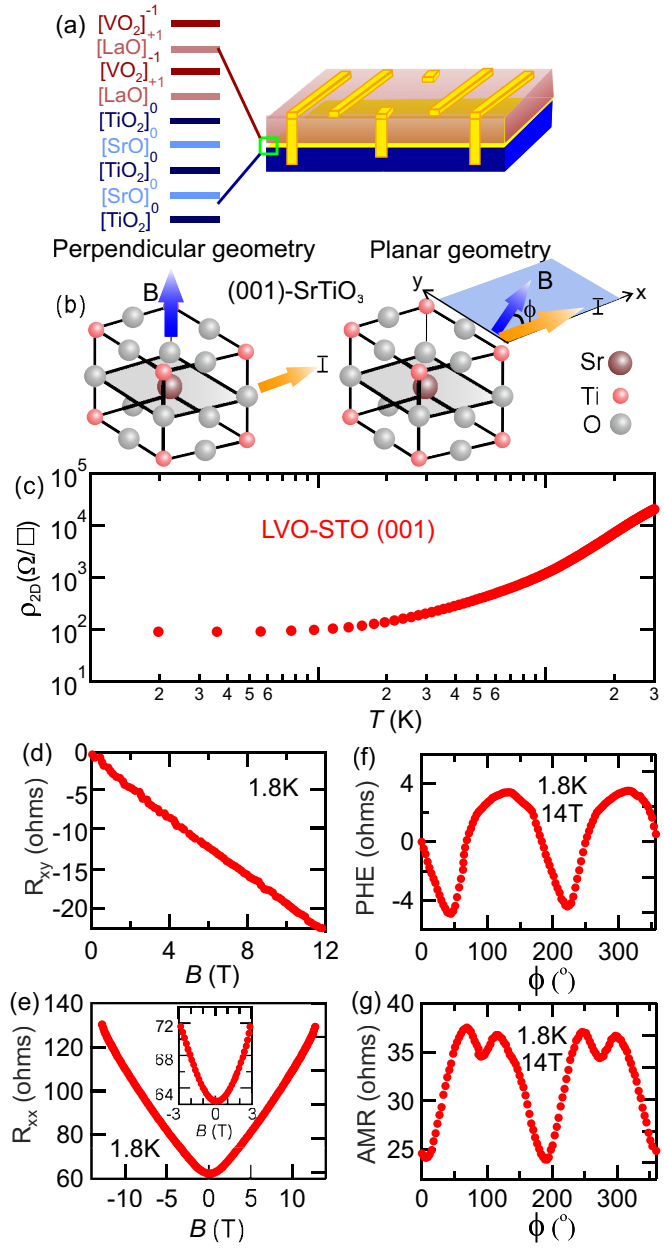

FIG. 1. (a) Schematic of the LVO/STO heterostructure with alternating planes in LVO and STO (001). (b) Schematic of the atomic configuration of (001) STO in perpendicular (left) and planar (right) geometries. (c) Temperature dependence of sheet resistivity in the (001) LVO/STO case. (d) R_{xy} and (e) R_{xx} measured in the perpendicular geometry as a function of magnetic field at 1.8 K. The inset in (e) shows the R_{xx} data in the low magnetic field range. (f) The PHE and (g) AMR measured in the planar geometry at 14 T and 1.8 K as a function of angle ϕ, respectively.

3.1×10^{14} cm^{-2} and 220 cm^2 V^{-1} s^{-1} at 1.8 K, respectively. Figures 1(d) and 1(e) show the transverse (R_{xy}) and longitudinal (R_{xx}) resistances when measured in the perpendicular geometry at 1.8 K, respectively. The linear nature of the Hall resistance with magnetic field confirms the presence of one type of charge carrier in the system, as can be seen in Fig. 1(d). The R_{xx} measurement shows the positive magnetoresistance (MR) at 1.8 K. The inset shows the MR for low magnetic field

values. No signature of weak antilocalization (WAL) is seen for this interface. On performing these measurements in the planar geometry, oscillations in transverse and longitudinal resistances are observed under application of magnetic field (data are shown at 14 T and a temperature of 1.8 K). These observed oscillations in transverse and longitudinal resistances are known as the planar Hall effect and anisotropic magnetoresistance, respectively. Figures 1(f) and 1(g) show the PHE and AMR measurements as a function of angle ϕ between the magnetic field and current direction, respectively.

Similar measurements were performed for the (111)-oriented interface of LVO/STO. Figure 2(a) shows the schematic of the LVO/STO heterostructure displaying alternating planes in LVO and STO with (111) orientation. The alternating charged planes in (111)-oriented STO are Ti^{4+} and $(SrO_3)^{4-}$; for LVO, the planes are $(LaO_3)^{3-}$ and V^{3+}. Figure 2(b) schematically represents the perpendicular (left) and planar (right) geometries of the measurements for the (111)-oriented LVO/STO heterostructure. This interface of (111)-oriented LVO/STO also shows a conducting nature [45] with a slight upturn in resistance at low temperature, similar to what was shown by Refs. [39,49]. The carrier density and mobility of this heterostructure were 7.5×10^{13} cm^{-2} and 152 cm^2 V^{-1} s^{-1} at 1.8 K, respectively. The difference in the charge carrier density at the (001) and (111) interface is not entirely new; similar behavior was already reported for LAO/STO interfaces [45,50]. The prerequisite to obtain a two-dimensional electron gas (2DEG) in (001) STO is a TiO_2-terminated surface of (001) STO through a charge reconstruction process. The proposed charge reconstruction model dopes 1/2 electron per unit cell (3.2×10^{14} cm^{-2} carrier density) [51,52]. Our (001) interface shows a very similar carrier density. However, observation of the 2DEG at the (111) LVO/STO interface gives us the freedom to suppress such restrictions to realize a 2DEG and could be a reason for the observed differences in carrier densities. Figures 2(d) and 2(e) show R_{xy} and R_{xx} measured in the perpendicular geometry at 1.8 K, respectively. The linear nature of the Hall resistance with magnetic field confirms the presence of one type of charge carrier, as can be seen in Fig. 2(d). Similar to the (001) interface, the R_{xx} measurement shows a positive MR at 1.8 K, but the signature of WAL was seen for this interface. The inset shows the MR for low magnetic field values. The oscillations in transverse and longitudinal resistances as a function of the angle between current and applied magnetic field are observed under the application of magnetic field (data at 14 T and 1.8 K are shown) when measurements were performed in the planar geometry. Figures 2(f) and 2(g) show the PHE and AMR measurements as a function of angle ϕ, respectively.

Regarding data reproducibility and sample stability, we prepared another two sets of both (001)- and (111)-oriented LVO/STO heterostructures under the same growth parameters. The measurements were performed in the perpendicular and planar geometries on these samples. We could see similar effects in these samples, which confirmed our data stability and reproducibility.

Further, we extended our study of AMR and PHE in both (001)- and (111)-oriented LVO/STO heterointerfaces, and magnetic field dependent measurements were carried out. Figures 3(a) and 3(b) show the AMR measured at 1.8 K as a

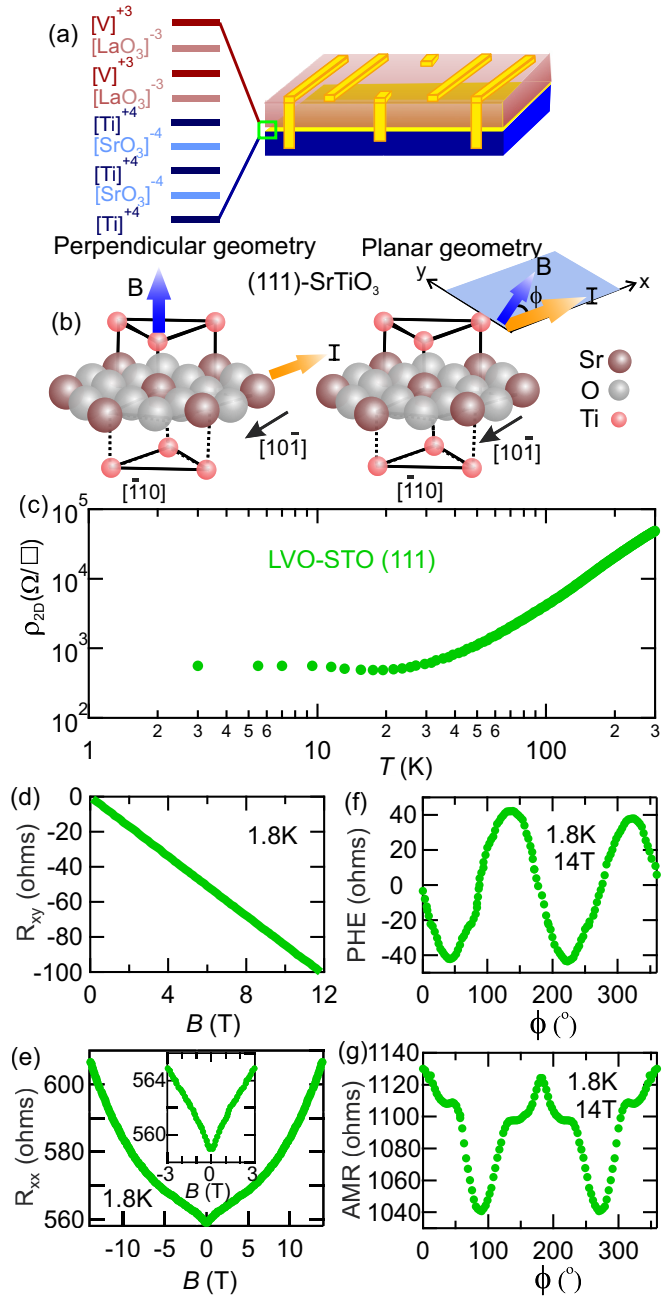

FIG. 2. (a) Schematic of the LVO/STO heterostructure with alternating planes in LVO and STO (111). (b) Schematic of the atomic configuration of (111) STO in perpendicular (left) and planar (right) geometries. (c) Temperature dependence of sheet resistivity in the (111) LVO/STO case. (d) R_{xy} and (e) R_{xx} measured in the perpendicular geometry as a function of magnetic field at 1.8 K. The inset in (e) shows the R_{xx} data in the low magnetic field range. (f) The PHE and (g) AMR measured in the planar geometry at 14 T and 1.8 K as a function of angle ϕ, respectively.

function of scan angle ϕ for both heterostructures. The applied various magnetic fields are given in the figures. To remove any artifacts, we symmetrized our data using [AMR (B,ϕ) + AMR $(-B,\phi)$]/2 → AMR (B,ϕ). A fourfold oscillation was seen in the (001) LVO/STO heterostructure, whereas sixfold oscillations were observed for (111)-oriented LVO/STO. For

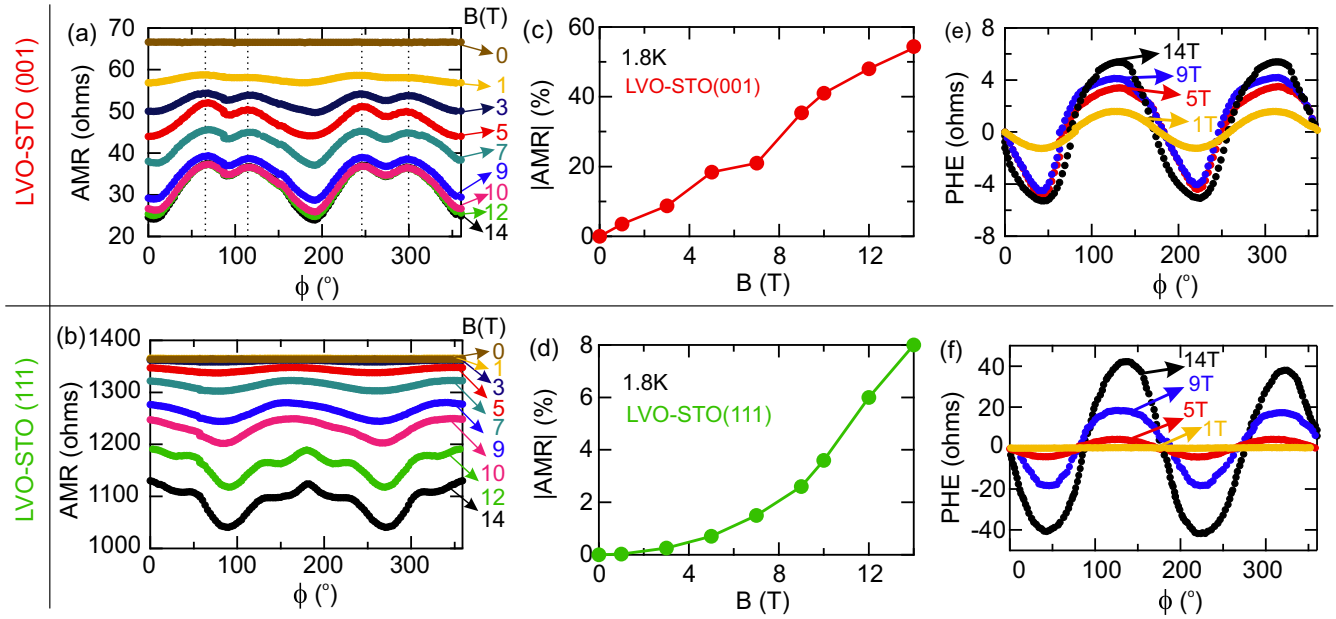

FIG. 3. Magnetic field dependent measurements. (a) and (b) AMR measurements measured at 1.8 K for the (001) and (111) LVO/STO heterointerfaces, respectively. (c) and (d) |AMR| (%) as a function of magnetic field at 1.8 K in both cases. (e) and (f) PHE measured at 1.8 K for different magnetic fields for the (001) and (111) LVO/STO heterostructures, respectively.

these measurements, the magnetic field is varied from 0 to 14 T. A clear decrease in the amplitude of oscillations on decreasing the magnetic field was observed in both AMR and PHE. The peaks in AMR appear at 70° and 115° (245° and 300°) with a small dip at 90° (270°). It is seen that in the case of (001)-oriented LVO/STO, the fourfold feature appearing in AMR persists even at low magnetic field (1 T). For the (111) case, the sixfold oscillation appears. On decreasing the magnetic field, these sixfold oscillations gradually transform into twofold oscillations with resistance maxima appearing at 0° and 180° with a periodicity of 180° and then completely vanish below a magnetic field of 5 T. The observed anisotropy in AMR for both interfaces, (001) and (111) LVO/STO, might be correlated with the orbital occupancy and Ti-site symmetries, as also discussed by Ma *et al.* for the LAO/STO (110) interface [39].

We calculated the percentage change in AMR at 1.8 K, which is defined as $|\text{AMR}|\ (\%) = |[R(\phi) - R(0)/R(0)]| \times 100$, for both heterointerfaces. Figures 3(c) and 3(d) show the plots for |AMR| (%) as a function of applied magnetic field for both cases. Higher change in resistance (∼60%) is observed in the case of (001)-oriented LVO/STO than in the (111) case (∼8%). The (001)-oriented LVO/STO heterointerface shows higher AMR than other oxide heterostructures such as LVO/KTO and LAO/STO with different orientations [14,32,35]. Figures 3(e) and 3(f) display the observed PHE with resistance minima at 45° and 225° at different magnetic field values for the (001)- and (111)-oriented LVO/STO interfaces, respectively. This shows that the amplitude of the PHE oscillations decreases with decreasing magnetic field. The sign change in the Hall signal with the angle ϕ variation between the current and magnetic field is the signature of PHE. The observed PHE in both cases remains twofold in nature, and no transformation in PHE oscillations was observed with decreasing magnetic field. It is also observed that PHE amplitude changes faster in (111) LVO/STO compared to (001) LVO/STO. Further experimental and theoretical study is required to understand this. Our experimental results suggest that four- and six- or twofold oscillation in AMR can be seen in such oxide systems, whereas the PHE shows only twofold oscillation. It was also observed that similar to AMR, the PHE oscillations persist at a low magnetic field of 1 T in the case of (001), whereas they vanish below 5 T in the (111) LVO/STO case. But unlike the higher AMR observed for (001) LVO/STO, the (111)-oriented LVO/STO shows a higher PHE amplitude change, as can be seen in Figs. 3(e) and 3(f).

Now, the question arises of what the possible origin of such effects observed in these heterointerfaces of LVO/STO could be. In (001) LAO/STO heterostructures, the origin of AMR is linked to the anisotropy in magnetic scattering arising from electron interaction with localized magnetic moments coupled to crystal symmetry [31]. In the case of our (001) and (111) LVO/STO systems, no evidence of magnetic ordering is seen in the transport measurements (such as the anomalous Hall effect), which rules out the possibility of magnetism-driven AMR observed in LVO/STO heterointerfaces. This points to the fact that the AMR and PHE observed in our systems might be related to their Fermi surface reconstruction due to orbital polarization/hybridization.

In both (001) and (111) LVO/STO heterointerfaces, an asymmetric component at high magnetic fields is observed in AMR [Figs. 3(a) and 3(b)], supporting the fact that the AMR could be related to orbital occupancies and crystal symmetries similar to those seen in the LAO/STO system and discussed by Rushforth *et al.* [39,53]. In addition, large AMR in the (001) interface is seen compared to that in the (111) interface of LVO/STO, as can be seen in Figs. 3(c) and 3(d). We observed behavior of AMR for the (001)- and (111)-oriented interfaces of LVO/STO similar to that observed for the LAO/STO (110)

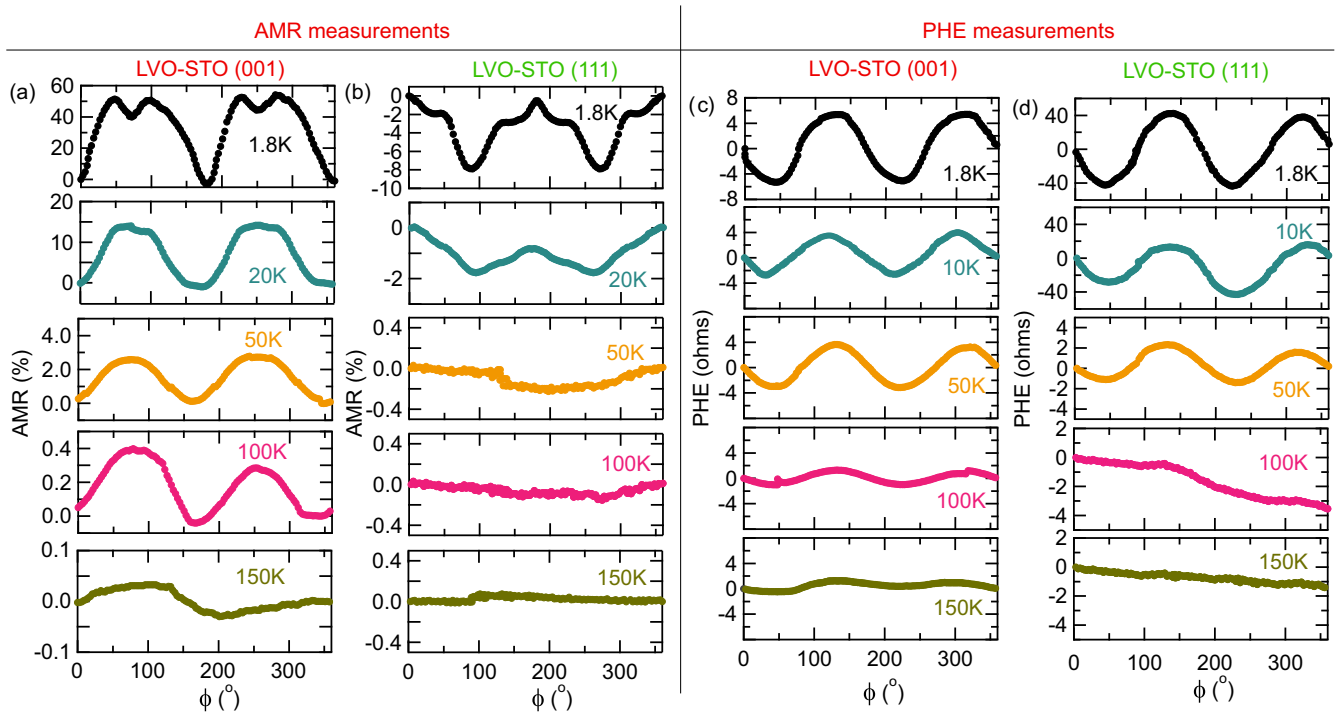

FIG. 4. Temperature-dependent (a) and (b) AMR measurements and (c) and (d) PHE measurements as a function of angle ϕ between current and magnetic field for (001)- and (111)-oriented LVO/STO heterostructures at 1.8 K, respectively.

interface, where the AMR is dominated by the crystalline term. In the case of the LAO/STO (110) interface, enlargement/suppression of the orbital shape along some specific directions indicated the orbital polarization and hybridization giving rise to giant crystalline AMR [39]. This was in contrast to (001) LAO/STO, where, usually, the noncrystalline term gives the dominant contribution to AMR [31,34]. In (001) LVO/STO, splitting in AMR peaks is observed at high magnetic fields, suggesting the contribution from polarized d_{xz}/d_{yz} orbitals [34,39]. Interestingly, this splitting is also observed in AMR when measured at low magnetic fields. Earlier studies showed that in the presence of small magnetic fields, only unpolarized d_{xy} orbitals within the inner side of the Brillouin zone contribute to AMR and normal AMR is seen. When the magnetic field strength is increased, the contribution from polarized d_{xz}/d_{yz} orbitals starts playing a role since at high magnetic fields, detection of Brillouin zone edges and electronic states becomes possible. This causes additional peaks in AMR at high fields, and this effect might be attributed to the multibands inducing different orbits at Fermi surfaces [39,54,55]. Our results for (001) LVO/STO for low magnetic fields indicate that the electrons near the Brillouin zone edges contribute to AMR, which gives rise to the splitting in AMR even at low magnetic field values.

In addition to the magnetic field dependent measurements, we have also investigated the effect of temperature on AMR and PHE measurements. Figure 4 shows the AMR [Figs. 4(a) and 4(b)] and PHE [Figs. 4(c) and 4(d)] measurements performed for both (001) and (111) LVO/STO heterostructures at 14 T with varying temperature. The amplitude of oscillations in AMR and PHE for both heterointerfaces decreases on increasing the temperature. The oscillations in AMR [Fig. 4(a)] and PHE [Fig. 4(c)] in the case of the (001)-oriented interface persist up to 150 K, and above this temperature, the oscillations disappear, which might be due to the emergence of thermal fluctuations at high temperature. However, the oscillations in AMR [Fig. 4(b)] and PHE [Fig. 4(d)] for (111)-oriented LVO/STO vanish at much lower temperature (∼20 K) compared to the (001) LVO/STO heterointerface (∼150 K). This observation suggests a strong effect of thermal fluctuations on AMR and PHE at the (111) interface of LVO/STO compared to the (001) interface. A similar observation was reported for LAO/STO heterostructures, where the oscillations in the longitudinal (AMR) and transverse (PHE) resistances disappear above 20 K due to thermal fluctuations emerging at high temperatures [31,32].

We plot the amplitudes of PHE (left axis) and AMR (right axis) in Figs. 5(a) and 5(b) as a function of applied magnetic field for (001)- and (111)-oriented interfaces of the LVO/STO system to check their dependence on magnetic field. In the case of (001) LVO/STO, it is seen that the PHE amplitude follows B^2 dependence, whereas the AMR amplitude deviates from it. On the other hand, the amplitude of PHE as well as AMR in the (111) interface follows B^2 dependence. Earlier reports suggested that the B^2 dependence of PHE and AMR might originate from either orbital magnetoresistance or a chiral anomaly, as seen in topological materials [23,26–30,56]. The origin of such magnetic field dependence is not clear in the present case. It is worth noting that our present experimental observations, especially the absence of negative longitudinal magnetoresistance, as well as theoretical simulations suggest that such magnetic field dependence of LVO/STO does not originate from the chiral anomaly observed in Dirac/Weyl semimetals; rather, it is most

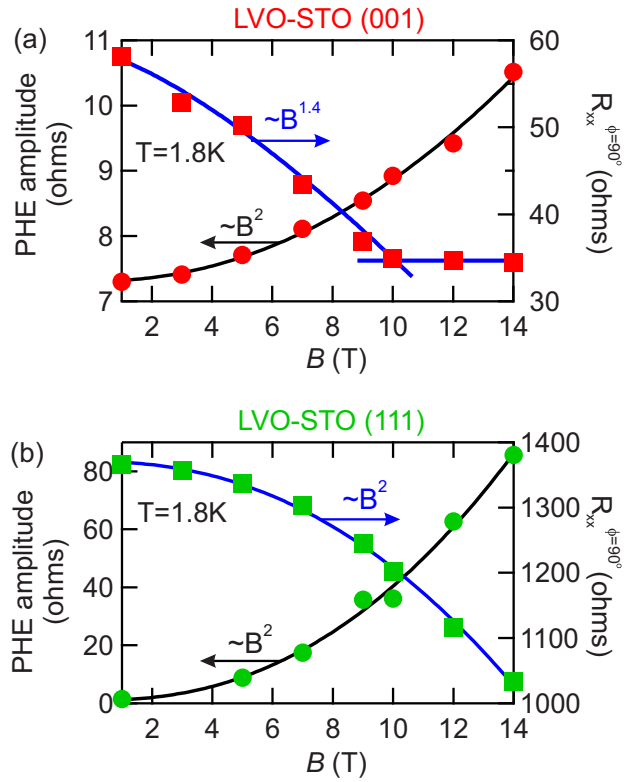

FIG. 5. (a) and (b) Left axis: PHE amplitudes; right axis: AMR amplitudes as a function of magnetic field for the (001) and (111) heterointerfaces of LVO/STO at 1.8 K, respectively.

likely generated by the orbital magnetoresistance and might be linked to the reconstruction of their unique Fermi surfaces [56]. To unambiguously identify the origin of magnetic field dependence further systematic theoretical as well as experimental studies should be performed in detail [28,57].

To check the nature (crystalline/noncrystalline) of the AMR further in our case of (001) and (111) LVO/STO, we employed symmetry considerations for 2D square and hexagonal crystals, as discussed by Rout *et al.* for the LAO/STO system [32]. In the case of (001) LVO/STO, we considered ϕ (θ) as the angle between the applied magnetic field (current) and the [001] crystal axis. However, ϕ (θ) is the angle between the applied magnetic field (current) and the [110] crystal axis for the (111) case. For 2D square and hexagonal crystals (when $\theta = 0$), the AMR and PHE can be expressed as

$$\mathrm{AMR}_{sq/hex} = C_2\cos 2\phi + C_4\cos 4\phi + C_6\cos 6\phi, \quad (1)$$

$$\mathrm{PHE}_{sq} = S_2\sin 2\phi + S_6\sin 6\phi, \quad (2)$$

$$\mathrm{PHE}_{hex} = C_2\sin 2\phi - C_4\sin 4\phi. \quad (3)$$

The contributing terms to the AMR are C_2 and S_2, C_4 and C_6, and S_6, corresponding to two-, four-, and sixfold AMRs, respectively. We have fitted our AMR data with the above equations to determine the role of fourfold and sixfold symmetries in (001) and (111) interfaces, respectively. The fitting analysis of AMR (left and middle panels) and PHE (right panels) for both interfaces is presented in Fig. 6. The AMR data observed for (001) and (111) LVO/STO interfaces are fitted using Eq. (1). It is seen [Fig. 6(a)] that the AMR data (at 14 T and 1.8 K) for (001) LVO/STO fit well with the fourfold component. However, the AMR data for (111) LVO/STO [Fig. 6(b); at 14 T and 1.8 K] have a sixfold component. The cyan line represents the fit curve. We have performed a similar analysis for the AMR data observed at low magnetic fields. The AMR data in the case of (111) fit well with only the twofold component, i.e., $C_2\cos 2\phi$ [the data at 5 T are shown

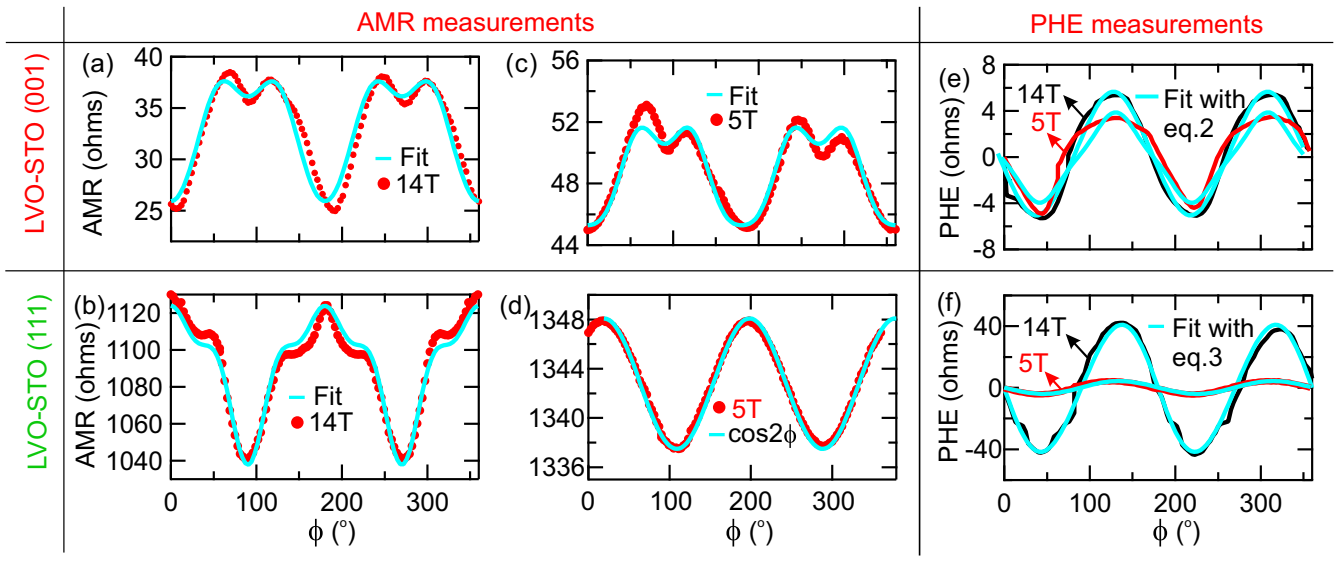

FIG. 6. (a) and (b) The AMR at 14 T and 1.8 K as a function of ϕ for the (001) and (111) LVO/STO interfaces, respectively. The cyan lines in (a) and (b) represent the fourfold and sixfold components, respectively. (c) The AMR data for (001) at low magnetic field (5 T and 1.8 K) also fit with the fourfold component. (d) In (111) LVO/STO, the AMR data at low magnetic field (5 T and 1.8 K) fit with the twofold component. The PHE at 1.8 K obtained at 14 and 5 T for (g) the (001) and (h) (111) LVO/STO heterointerfaces, which fit well with Eqs. (2) and (3).

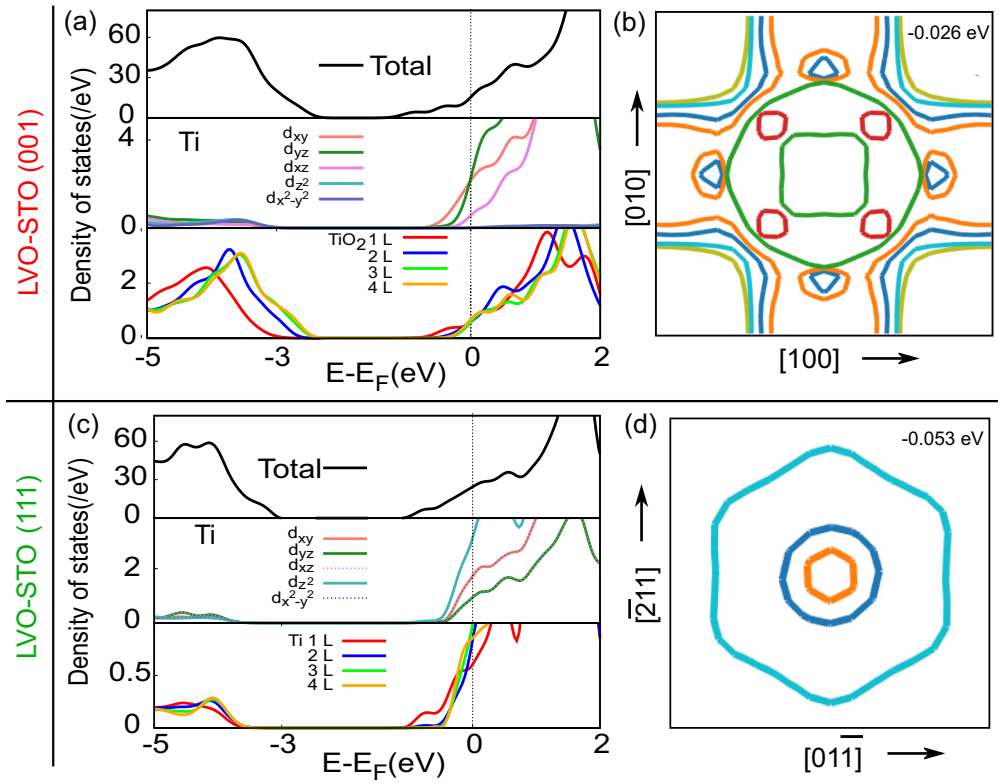

FIG. 7. The total DOS and DOS projected onto 3*d* orbitals of Ti atoms as well as the contribution from layers as we move away from the interface, calculated by DFT for LVO/STO heterostructures in (a) the (001) and (c) (111) orientations with the layers numbered from 1 to 4 as we move away from the interface. Calculated Fermi surface plots of the LVO/STO (b) (001) and (d) (111) heterostructures in the (001) and (111) planes, respectively, with colors representing the different bands.

in the Fig. 6(d)]. However, the AMR data observed at low magnetic fields [5 T data are shown in Fig. 6(c)] in (001) LVO/STO fit with the fourfold component. A detail analysis of AMR data for both heterostructures is discussed in the Supplemental Material (Figs. S2 and S3). Figures 6(e) and 6(f) show that similar to AMR, the PHE observed for both interfaces also fits well with the Eqs. (2) and (3), displaying good agreement with the calculated AMR and PHE for 2D square and hexagonal crystals. Our fitting analysis suggests that the data for both (001) and (111) LVO/STO interfaces show four and sixfold behaviors, respectively. They follow the cos4ϕ and cos6ϕ law, as expected for square and 2D hexagonal systems, thus indicating that the AMR is related to the crystal symmetries of the systems for both interfaces.

IV. THEORETICAL CALCULATIONS

To explore the origin of observed AMR and PHE in LVO/STO heterostructures with (001) and (111) orientations, first-principles calculations based on density functional theory (DFT) were performed as implemented within the VASP (Vienna Ab initio Simulation Package) code. To account for exchange-correlation effects the Perdew-Burke-Ernzerhof functional revised for solids (PBEsol) was used within the generalized-gradient approximation [58] with projector augmented wave potentials [59,60]. A kinetic energy cutoff of 520 eV was used for the plane wave basis [61]. For relaxation and static calculations, the Brillouin zone was sampled with a 6×6×1 Γ-centered *k*-point grid. For density of states (DOS) calculations a 10×10×1 *k*-point mesh was used. To simulate the interfaces, a stoichiometric thin film model with a LVO thin film on an STO substrate with vacuum on top of LVO was considered. The interface was modeled with four layers of LVO attached to nine layers of STO with a TiO_2/LaO (Ti/LaO_3) interface for the (001) [(111)] orientation. We employed thin-film geometry with a vacuum region of 15 Å to avoid the interaction between adjacent slabs. To account for the electronic correlation between localized electrons of 3*d* orbitals of Ti and V and to correct the on-site Coulomb interaction, DFT+U calculations were performed using Dudarev's rotationally invariant approach (where only $U - J$ is meaningful) [62]. Here, U is the effective on-site Coulomb interaction between localized 3*d* electrons (Hubbard's U), and J is the exchange parameter. Values of $U = 5$ eV, $J = 0.64$ eV were used for the Ti atom, and $U = 3$ eV, $J = 0$ eV were used for the V atom.

The origin of experimental findings for the AMR and PHE in the (001) orientation is explored by a density of states plot. In Fig. 7(a), we show the total DOS as well as the DOS projected onto 3*d* orbitals of Ti atoms to get information about the relative *d*-orbital occupancy at the Fermi level as well as in valence and conduction band regions. The total DOS verifies the *n*-type metallic nature of this conducting heterointerface of two oxide materials which are insulators in the bulk with valence and conduction bands separated by a gap. The DOS projected onto 3*d* orbitals of Ti atoms implies

that electrons responsible for conductivity occupy d_{yz} and d_{xz} orbitals which hybridize to give orbital polarization along the z axis, and the effect is slightly reduced by d_{xy} orbitals. We also plot the density of states showing the contribution from layers containing Ti atoms, viz., the first four TiO_2 planes with the layers numbered from 1 to 4 as we move away from the interface in Fig. 7(a). Also, the degeneracy between d_{yz} and d_{xz} orbitals for the (001) orientation is broken, which leads to splitting in AMR peaks, as observed experimentally. Experimental AMR data show fourfold oscillations at high as well as low values of magnetic field. This can be further explained by the Fermi surface of the LVO/STO heterointerface calculated in the (001) plane for the (001) orientation. We used the value of the Fermi energy equal to the chemical potential corresponding to the carrier concentration measured experimentally. The Fermi surface plot as shown in Fig. 7(b) reveals fourfold symmetry due to the crystal structure in the (001) orientation. We infer that open orbits present in this case give rise to prominent splitting in AMR peaks as observed at magnetic fields in experimental measurements. This is due to the fact that at these values of magnetic field, electrons present near the edge of the Brillouin zone can be detected where these open orbits are present, in contrast to the detection of electrons present only near the center of the Brillouin zone at very low fields.

Similar calculations for the LVO/STO heterostructure with the (111) orientation for the DOS in Fig. 7(c) show the conduction band crossing the Fermi level and valence band separated by a gap, thus revealing n-type conducting behavior. Further, the DOS projected onto $3d$ orbitals of Ti atoms shows that the contribution to electronic states at the Fermi level comes from d_{z^2} and degenerate d_{yz} and d_{xz} orbitals. This gives rise to orbital polarization along the z axis, which is the (111) direction (crystal orientation) in this instance, similar to the case of the (001)-oriented heterostructure. But the contribution coming from degenerate d_{xy} and $d_{x^2-y^2}$ orbitals greatly dilutes this effect of orbital polarization along the z axis, which is responsible for the weaker or reduced effect in this case compared to the (001) orientation. This explains why AMR and PHE persist at 1 T for the (001) heterostructure but vanish below 5 T for the (111) orientation or AMR and PHE persist up to 150 K for the (001) orientation and vanish at 20 K for the (111)-oriented heterostructure. We plot the density of states showing the contribution of the first four Ti planes with the layers numbered from 1 to 4 as we move away from the interface in Fig. 7(c), indicating that the metallic partial DOS goes deep into the bulk of STO. Further, the Fermi surface calculated for the LVO/STO heterostructure with the (111) orientation in the (111) plane at a Fermi energy equal to the chemical potential corresponding to the experimental value of the carrier concentration [Fig. 7(d)] shows sixfold symmetry as well as an absence of open orbits in this case and hence justifies the absence of peak splitting. Our theoretical simulations for both heterointerfaces suggest that the orbital polarization/hybridization along with the orbital occupancy leads to the reconstruction of their Fermi surfaces, resulting in the oscillations in the longitudinal (AMR) and transverse (PHE) resistances of the heterointerfaces with the peculiar features.

V. CONCLUSION

In conclusion, we have realized the conducting interfaces of (001)- and (111)-oriented LVO/STO systems. We observed the signature of WAL only in the (111) LVO/STO interface. The in-plane magnetotransport measurements showed the oscillations in longitudinal (AMR) and transverse (PHE) magnetoresistances for both interfaces. Fourfold oscillation was observed in the (001) LVO/STO interface, whereas the (111) LVO/STO showed sixfold oscillation which further transformed into twofold oscillation with a decrease in magnetic field. Higher AMR (∼60%) is observed in (001) LVO/STO compared to the (111) interface and is the highest among reported oxide heterointerfaces. Also, these oscillations in AMR and PHE persist up to higher temperature in the case of (001) LVO/STO (∼150 K) than in the (111) case (∼20 K) and LAO/STO (above 20 K), suggesting a reduced effect of thermal fluctuations in (001) LVO/STO. The fitting analysis of AMR for both interfaces suggested the AMR is related to the crystal symmetries of the systems. From the DFT simulations, we have observed the orbital polarization and hybridization in both interfaces, which is less strong for the (111) system. Also, it is evident that the presence of open orbits in the Fermi surface plot calculated in the reciprocal space of (001)-oriented system explains the splitting of AMR peaks in (001) LVO/STO. Our theoretical calculations, with the support of our experimental results, suggest that the origin of these oscillations in AMR and PHE can be attributed to their unique Fermi surface reconstruction due to orbital occupancy and polarization/hybridization in both (001) and (111) heterostructures.

ACKNOWLEDGMENTS

S.C. and R.T. acknowledge the financial support from the Department of Science and Technology (DST), India, Nano Mission Project No. SR/NM/NS-1007/2015. Also, we acknowledge that this work would not have been possible without the combinatorial pulsed laser deposition system sponsored by DST-Nano Mission at NPDL, INST, Mohali, India.

[1] S. Shigehiko, S. Junji, N. Kazuo, I. Tomonori, and H. Satoshi, Jpn. J. Appl. Phys. **23**, L573 (1984).
[2] T. Y. Lee, J. Chang, M. C. Hickey, H. C. Koo, H. J. Kim, S. H. Han, and J. S. Moodera, Appl. Phys. Lett. **98**, 202504 (2011).
[3] A. Ohtomo and H. Y. Hwang, Nature **427**, 423 (2004).
[4] S. Thiel, G. Hammerl, A. Schmehl, C. W. Schneider, and J. Mannhart, Science **313**, 1942 (2006).
[5] N. Nakagawa, H. Y. Hwang, and D. A. Muller, Nat. Mater. **5**, 204 (2006).
[6] R. Tomar, R. M. Varma, N. Kumar, D. D. Sarma, D. Maryenko, and S. Chakraverty, Adv. Mater. Inter. **7**, 1900941 (2019).
[7] J. Biscaras, N. Bergeal, A. Kushwaha, T. Wolf, A. Rastogi, R. C. Budhani, and J. Lesueur, Nat. Commun. **1**, 89 (2010).
[8] K. Zou, S. I. Beigi, K. Kisslinger, X. Shen, D. Su, F. J. Walker, and C. H. Ahn, APL Mater. **3**, 036104 (2015).

[9] J. Betancourt, T. R. Paudel, E. Y. Tsymbal, and J. P. Velev, Phys. Rev. B **96**, 045113 (2017).

[10] J. S. Lee, Y. W. Xie, H. K. Sato, C. Bell, Y. Hikita, H. Y. Hwang, and C. C. Cao, Nat. Mater. **12**, 703 (2013).

[11] J. F. Schooley, W. R. Hosler, and M. L. Cohen, Phys. Rev. Lett. **12**, 474 (1964).

[12] L. Li, C. Richter, J. Mannhart, and R. C. Ashoori, Nat. Phys. **7**, 762 (2011).

[13] A. D. Caviglia, M. Gabay, S. Gariglio, N. Reyren, C. Cancellieri, and J. M. Triscone, Phys. Rev. Lett. **104**, 126803 (2010).

[14] N. Wadehra, R. Tomar, R. M. Varma, R. K. Gopal, Y. Singh, S. Dattagupta, and S. Chakraverty, Nat. Commun. **11**, 874 (2020).

[15] N. Kumar, N. Wadehra, R. Tomar, S. Dattagupta, S. Kumar, and S. Chakraverty, Adv. Quantum Technol. **4**, 2000081 (2020).

[16] W. Thomson, Proc. R. Soc. **8**, 546 (1857).

[17] W. Doring, Ann. Phys. **424**, 259 (1938).

[18] R. P. van Gorkom, J. Caro, T. M. Klapwijk, and S. Radelaar, Phys. Rev. B **63**, 134432 (2001).

[19] P. N. Hai, D. Sasaki, L. D. Anh, and M. Tanaka, Appl. Phys. Lett. **100**, 262409 (2012).

[20] V. D. Ky, Phys. Status Solidi **26**, 565 (1968).

[21] S. T. B. Goennenwein, R. S. Keizer, S. W. Schink, I. V Dijk, T. M. Klapwijk, G. X. Miao, G. Xiao, and A. Gupta, Appl. Phys. Lett. **90**, 142509 (2007).

[22] M. Trushin, K. Vyborny, P. Moraczewski, A. A. Kovalev, J. Schliemann, and T. Jungwirth, Phys. Rev. B **80**, 134405 (2009).

[23] A. A. Taskin, H. F. Legg, F. Yang, S. Sasaki, Y. Kanai, K. Matsumoto, A. Rosch, and Y. Ando, Nat. Commun. **8**, 1340 (2017).

[24] D. Rakhmilevich, F. Wang, W. Zhao, M. H. W. Chan, J. S. Moodera, C. Liu, and C. Z. Chang, Phys. Rev. B **98**, 094404 (2018).

[25] D. Ma, H. Jiang, H. Liu, and X. C. Xie, Phys. Rev. B **99**, 115121 (2019).

[26] R. Singha, S. Roy, A. Pariari, B. Satpati, and P. Mandal, Phys. Rev. B **98**, 081103(R) (2018).

[27] A. A. Burkov, Phys. Rev. B **96**, 041110(R) (2017).

[28] S. Nandy, G. Sharma, A. Taraphder, and S. Tewari, Phys. Rev. Lett. **119**, 176804 (2017).

[29] N. Kumar, S. N. Guin, C. Felser, and C. Shekhar, Phys. Rev. B **98**, 041103(R) (2018).

[30] S. Nandy, A. Taraphder, and S. Tewari, Sci. Rep. **8**, 14983 (2018).

[31] A. Annadi, Z. Huang, K. Gopinadhan, X. R. Wang, A. Srivastava, Z. Q. Liu, H. H. Ma, T. P. Sarkar, T. Venkatesan, and Ariando, Phys. Rev. B **87**, 201102(R) (2013).

[32] P. K. Rout, I. Agireen, E. Maniv, M. Goldstein, and Y Dagan, Phys. Rev. B **95**, 241107(R) (2017).

[33] A. Joshua, S. Pecker, J. Ruhman, E. Altman, and S. Ilani, Nat. Commun. **3**, 1129 (2012).

[34] A. Joshua, J. Ruhman, E. Altman, S. Pecker, and S. Ilani, Proc. Natl. Acad. Sci. USA **110**, 9633 (2013).

[35] K. Narayanapillai, K. Gopinadhan, X. Qiu, A. Annadi, Ariando, T. Venkatesan, and H. Yang, Appl. Phys. Lett. **105**, 162405 (2014).

[36] M. J. Jin, S. I. Kim, S. Y. Moon, S. Choe, J. Park, V. Modepalli, J. JO, I. Oh, S. H. Baek, and J. W. Yoo, J. Eletcron. Mater. **48**, 1347 (2018).

[37] A. Fete, S. Gariglio, A. D. Caviglia, J. M. Triscone, and M. Gabay, Phys. Rev. B **86**, 201105(R) (2012).

[38] E. Flekser, M. Ben Shalom, M. Kim, C. Bell, Y. Hikita, H. Y. Hwang, and Y. Dagan, Phys. Rev. B **86**, 121104(R) (2012).

[39] H. J. H. Ma, J. Zhou, M. Yang, Y. Liu, S. W. Zeng, W. X. Zhou, L. C. Zhang, T. Venkatesan, Y. P. Feng, and Ariando, Phys. Rev. B **95**, 155314 (2017).

[40] Y. Hotta, T. Susaki, and H. Y. Hwang, Phys. Rev. Lett. **99**, 236805 (2007).

[41] N. Wadehra, R. Tomar, Y. Yokoyama, A. Yasui, E. Ikenaga, H. Wadati, S. Maryenko, and S. Chakraverty, arXiv:2012.07191.

[42] R. Tomar, N. Wadehra, V. Budhiraja, B. Prakash, and S. Chakraverty, Appl. Surf. Sci. **427**, 861 (2017).

[43] See Supplemental Material at http://link.aps.org/supplemental/10.1103/PhysRevB.103.115407 for the fabrication of $LaVO_3$/$SrTiO_3$ heterostructure and fitting analysis of observed AMR.

[44] Y. Yamada, H. K. Sato, Y. Hikita, H. Y. Hwang, and Y. Kanemitsu, Appl. Phys. Lett. **104**, 151907 (2014).

[45] G. Herranz, F. Sanchez, M. Scigaj, and J. Fontcuberta, Sci. Rep. **2**, 758 (2012).

[46] S. Gariglio, M. Gabay, and J.-M. Triscone, APL Mater. **4**, 060701 (2016).

[47] A. M. R. V. L. Monteiro, D. J. Groenendijk, I. Groen, J. de Bruijckere, R. Gaudenzi, H. S. J. van der Zant, and A. D. Caviglia, Phys. Rev. B **96**, 020504(R) (2017).

[48] D. Doennig, W. E. Pickett, and R. Pentcheva, Phys. Rev. Lett. **111**, 126804 (2013).

[49] K. Han, N. Palina, S. W. Zeng, Z. Huang, C. J. Li, W. X. Zhou, D. Y. Wan, S. W. Zeng, L. C. Zhang, X. Chi, R. Guo, J. S. Chan, T. Venkatesan, A. Rusydi, and Ariando, Sci. Rep. **6**, 25455 (2016).

[50] G. Z Liu, J. Q. Chen, Y. C. Jiang, R. Zao, J. Qiu, and J. Gao, J. Phys. D **53**, 095303 (2020).

[51] N. T. Trang, T. V. Nam, P. B. Duy, and G. H. Bach, J. Phys.: Conf. Ser. **537**, 012007 (2014).

[52] P. Delugas, A. Filippetti, V. Fiorentini, D. I. Bilc, D. Fontaine, and P. Ghosez, Phys. Rev. Lett. **106**, 166807 (2011).

[53] A. W. Rushforth, K. Výborný, C. S. King, K. W. Edmonds, R. P. Campion, C. T. Foxon, J. Wunderlich, A. C. Irvine, P. Vasek, V. Novak, K. Olejník, J. Sinova, T. Jungwirth, and B. L. Gallagher, Phys. Rev. Lett. **99**, 147207 (2007).

[54] G. Herranz, G. Singh, N. Bergeal, A. Jouan, J. Lesueur, J. Gazquez, M. Varela, M. Scigaj, N. Dix, F. Sanchez, and J. Fontcuberta, Nat. Commun. **6**, 6028 (2015).

[55] M. Salluzzo, J. C. Cezar, N. B. Brookes, V. Bisogni, G. M. D. Luca, C. Richter, S. Thiel, J. Mannhart, M. Huijben, A. Brinkman, G. Rijnders, and G. Ghiringhelli, Phys. Rev. Lett. **102**, 166804 (2009).

[56] Q. Liu, F. Fei, B. Chen, X. Bo, B. Wei, S. Zhang, M. Zhang, F. Xie, M. Naveed, X. Wan, F. Song, and B. Wang, Phys. Rev. B **99**, 155119 (2019).

[57] Z. Li, T. Xiao, R. Zou, J. Li, Y. Zhang, Y. Zeng, M. Zhou, J. Zhang, and W. Wu, J. Appl. Phys. **127**, 054306 (2020).

[58] J. P. Perdew, K. Burke, and M. Ernzerhof, Phys. Rev. Lett. **77**, 3865 (1996).

[59] G. Kresse and D. Joubert, Phys. Rev. B **59**, 1758 (1999).

[60] P. E. Blöchl, Phys. Rev. B **50**, 17953 (1994).

[61] G. Kresse and J. Furthmüller, Phys. Rev. B **54**, 11169 (1996).

[62] S. L. Dudarev, G. A. Botton, S. Y. Savrasov, C. J. Humphreys, and A. P. Sutton, Phys. Rev. B **57**, 1505 (1998).